

## Nanosecond Dynamics of Ferroelectric/Dielectric Superlattices

Ji Young Jo,<sup>1,\*</sup> Pice Chen,<sup>1</sup> Rebecca J. Sichel,<sup>1</sup> Sara J. Callori,<sup>2</sup> John Sinsheimer,<sup>2</sup>  
Eric M. Dufresne,<sup>3</sup> Matthew Dawber,<sup>2</sup> and Paul G. Evans<sup>1,†</sup>

<sup>1</sup>*Department of Materials Science and Engineering and Materials Science Program,  
University of Wisconsin–Madison, Madison, Wisconsin 53706, USA*

<sup>2</sup>*Department of Physics and Astronomy, Stony Brook University, Stony Brook, New York 11794, USA*

<sup>3</sup>*Advanced Photon Source, Argonne National Laboratory, Argonne, Illinois 60439, USA*

(Received 15 April 2011; published 25 July 2011)

The nanosecond response of a  $\text{PbTiO}_3/\text{SrTiO}_3$  ferroelectric/dielectric superlattice to applied electric fields is closely linked to the dynamics of striped domains of the remnant polarization. The intensity of domain satellite reflections observed with time-resolved x-ray microdiffraction decays in 5–100 ns depending on the magnitude of the electric field. The piezoelectric response of the superlattice within stripe domains is strongly suppressed due to electromechanical clamping between adjacent regions of opposite polarization. Regions of the superlattice that have been switched into a uniform polarization state by the applied electric field, however, exhibit piezoelectricity during the course of the switching process. We propose a switching model different from previous models of the switching of superlattices, based instead on a spatially heterogeneous transformation between striped and uniform polarization states.

DOI: 10.1103/PhysRevLett.107.055501

PACS numbers: 61.05.cp, 77.55.Px, 77.80.Dj

Ferroelectric/dielectric superlattices have intriguing electronic and structural properties arising from the nanoscale interaction of ferroelectric polarization, crystallographic symmetry, and epitaxially imposed strain [1–7]. Electrostatic boundary conditions at the multitude of ferroelectric/dielectric interfaces within the superlattice result in the extension of the spontaneous polarization into the dielectric component. The spontaneous polarization is not perfectly screened by interfaces with electrodes or air, leading to the formation of  $180^\circ$  stripe polarization nanodomains [8–10]. Features such as the period of the stripe domain pattern are determined by the complex series of contributions to the energy of the superlattice including the electrostatic effects arising from uncompensated charges and the mechanical stress applied by the substrate [11,12]. External electric fields perturb this energy landscape and can result in a transformation of the stripe pattern to a uniform polarization. Theoretical studies have yielded a range of predictions, including that the polarization of the ferroelectric and dielectric components have different dynamic responses [8]. Experiments probing the structural response of ferroelectric/dielectric superlattices have been limited to slow time scales of milliseconds to seconds and have not captured the dynamical aspects of the superlattice response [9,13].

Nanosecond switching phenomena in uniformly polarized ferroelectrics are accurately described by models of the nucleation of domains with reversed polarization and the subsequent motion of domain walls [14,15]. Far less is known about the transition from striped nanodomains to uniform polarization in a ferroelectric/dielectric superlattice. In this Letter, we describe the structural response of superlattices at the nanosecond time scale, based on a

time-resolved x-ray microdiffraction study. We show that the dynamics of the superlattice as a whole is connected to the evolution of the striped domains, which occurs at a rate that depends on the magnitude of the applied electric field. We also show that piezoelectric expansion within striped domains is effectively clamped, as has been predicted for  $180^\circ$  domain walls in ferroelectrics [16], and thus differs from the average piezoelectricity of the regions of the superlattice that have reached the uniform polarization state. We thus propose that the transformation occurs by a heterogeneous switching model, distinct from the simple motion of domain walls, based instead on the conversion of areas of the film to the uniform polarization state.

A superlattice with a repeating unit consisting of 12 unit cells of  $\text{PbTiO}_3$  and 3 unit cells of  $\text{SrTiO}_3$ , with a total thickness of  $\sim 100$  nm, was deposited on a (001)-oriented  $\text{SrRuO}_3/\text{SrTiO}_3$  substrate using off-axis rf magnetron sputtering [17]. Pt top electrodes with a diameter of  $50 \mu\text{m}$  allowed an electric field to be applied along the surface normal; the  $\text{SrRuO}_3$  (SRO) layer, with a thickness of  $\sim 20$  nm, served as a continuous bottom electrode. X rays with photon energy of 10 keV were focused to a 200 nm spot using a Fresnel zone plate at station 7ID-B of the Advanced Photon Source. A gated area detector (Pilatus 100K, Dectris Ltd.) acquired the distribution of scattered intensity in reciprocal space [18]. During acquisition, electric-field pulses were repeated at a rate of 18 kHz and synchronized to the storage ring with a variable delay [19]. The area detector was gated to measure the diffracted intensity arising from x-ray bunches with the desired timing relationship to the applied field, i.e., at a specified time before or after the beginning of the electric-field pulse. The piezoelectric response of the superlattice was

used to synchronize the x-ray and electric-field pulses [20]. Time-resolved diffraction patterns were accumulated by using thousands to millions of electric-field pulses to achieve sufficient counting statistics.

The zero-field three-dimensional distribution of diffracted intensity in reciprocal space was reconstructed by using a large number of two-dimensional diffraction patterns. Figure 1(a) shows a planar section through reciprocal space at  $Q_x = 0$ . Here  $Q_i$  with  $i = x, y, \text{ or } z$  are components of the scattering wave vector along the axes inset in Fig. 1(a). The section of reciprocal space in Fig. 1(a) includes a series of reflections arising from the periodicity of the superlattice along  $z$ . Domain satellite reflections appear at the same  $Q_z$  as the superlattice reflections, with a nonzero  $Q_y$  component arising from periodicity of the

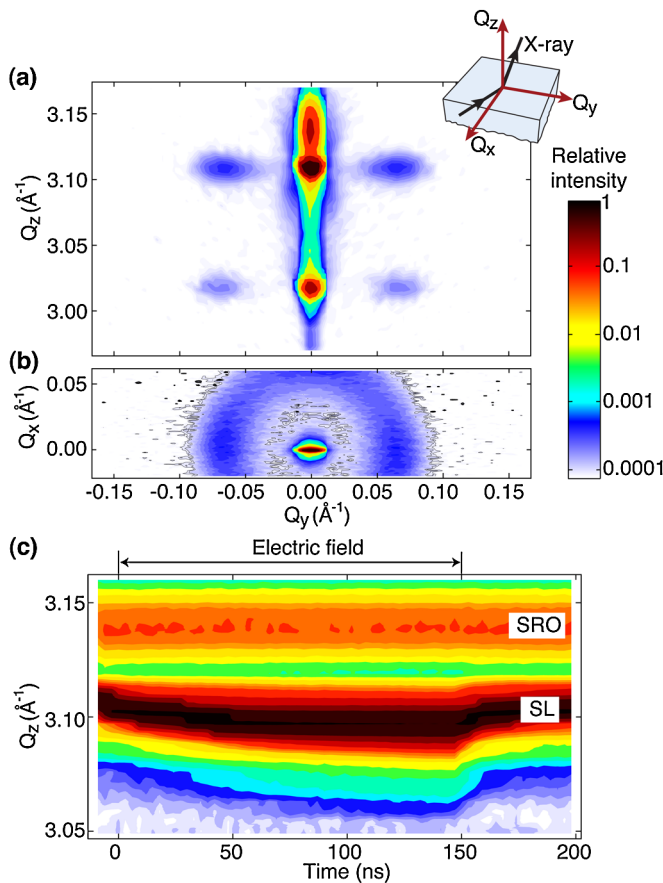


FIG. 1 (color online). Diffracted intensity in planar sections through reciprocal space at (a)  $Q_x = 0$  and (b)  $Q_z = 3.106 \text{ \AA}^{-1}$ . The intense feature at  $Q_z = 3.106 \text{ \AA}^{-1}$  arises from the (002) Bragg reflection of the average spacing of the superlattice. Reflections from the stripe nanodomains are apparent at nonzero values of  $Q_y$  in (a) and as a ring in the  $Q_x$ - $Q_y$  plane in (b). The inset shows a schematic of the scattering geometry. (c) The time dependence of the superlattice reflection at  $Q_z = 3.106 \text{ \AA}^{-1}$  during electric field with a magnitude of 0.84 MV/cm applied during the indicated interval. A reflection arising from the SRO bottom electrode appears in (a) and (c) at  $Q_z \approx 3.14 \text{ \AA}^{-1}$ . The color scale is labeled with intensities relative to the superlattice structural reflection.

in-plane stripe domain structure. Superlattice structural reflections along  $Q_y = 0$  have peak intensities approximately a factor of 2000 higher than the intensities of the corresponding domain reflections. Based on the reciprocal-space position and width determined from Fig. 1(a), the stripes have a period of 9.5 nm and a coherence length of 20 nm. Figure 1(b) shows a planar section of reciprocal space with  $Q_z = 3.106 \text{ \AA}^{-1}$ , so that the section passes through the intense superlattice reflection visible in Fig. 1(a). The intensity in the domain satellite reflections is distributed in a ring of constant radius around the  $z$  axis, for which the ratio of the intensities in the strongest and weakest directions is approximately two. We thus deduce that the stripe domains have nearly random in-plane orientations. The time scale associated with the response to external electric fields can be determined by using the piezoelectric shift of the superlattice reflection to smaller  $Q_z$ . Figure 1(c) shows that the expansion occurs over approximately 100 ns during a 150 ns-duration 0.84 MV/cm applied field, with a piezoelectric coefficient of 36 pm/V.

The changes of the domain structure induced by an applied electric field were probed by using the time dependence of the domain satellite reflections. To simplify the analysis, the electric field is treated as uniform in both the vertical and lateral directions. Figure 2(a) shows a diffraction pattern acquired near (002) superlattice reflection during a 150 ns-duration 1.06 MV/cm electric-field pulse,

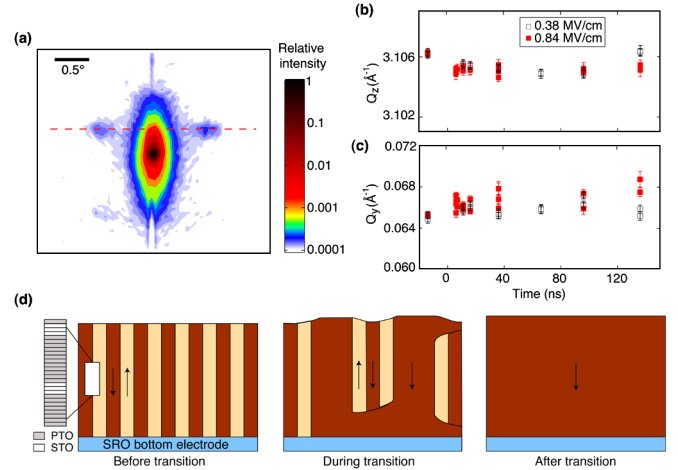


FIG. 2 (color online). (a) Diffraction pattern exhibiting superlattice and domain reflections, recorded in an applied electric field of 1.06 MV/cm with the diffractometer optimized for the superlattice reflection at  $Q_z = 3.085 \text{ \AA}^{-1}$ . The projection of the  $Q_z$  axis onto this diffraction pattern is along the vertical axis of the figure. The dashed line indicates the zero-field position of the superlattice reflection. (b)  $Q_z$  and (c)  $Q_y$  components of the wave vector of the domain reflection as a function of the time during applied electric fields of 0.38 and 0.84 MV/cm. (d) Domain patterns before, during, and after the transition from striped nanodomains to homogeneous uniform polarization. The in-plane coherence length of the striped pattern is drawn as infinite in order to simplify the representation. The sequence of atomic unit cells in the superlattice is shown as an inset.

from which the intensity and reciprocal-space position of the domain reflection can be determined. The  $Q_z$  and  $Q_y$  wave vectors of domain reflections are shown in Figs. 2(b) and 2(c) for two magnitudes of the applied electric field. The domain reflections exhibit a negligible change in  $Q_z$  during the electric-field pulses, which shows that piezoelectricity within the stripe domain is strongly suppressed. We attribute the absence of piezoelectric expansion in the domain satellites to electromechanical clamping, which allows the system to avoid the high elastic energy cost of a discontinuity of the lattice constant at domain walls [16]. We consistently observed no piezoelectric shift of the stripe domain reflection for any amplitude of the applied field. As shown in Fig. 2(c), the  $Q_y$  component of the domain reflection also remained unchanged under various electric fields, in agreement with the field independence of the in-plane periodicity reported in Ref. [9].

Zubko *et al.* interpreted long-time-scale x-ray diffraction measurements of domain reflections using a model in which the volume fraction of the favorable polarization increases via a continuous displacement of each domain boundary in the stripe pattern [9]. In this continuous-displacement model, piezoelectric distortion would develop in the domain reflection at the same rate at which it appears in the superlattice reflections. Our experimental observations, however, are incompatible with this prediction of the continuous-displacement model. Domain reflections, which do not exhibit piezoelectric expansion, are found at the same times at which expansion is evident in structural superlattice reflections. In a second model, Lisenkov, Ponomareva, and Bellaiche predict that remnant polarization in the dielectric component is switched earlier than in the ferroelectric component because the electrostatic energy required to switch the dielectric component is lower due to its slightly smaller polarization [8]. We anticipate that if the polarization of the dielectric component is switched in the manner proposed in Ref. [8], then the domain reflection would be shifted along  $Q_z$ , due to the accommodation of the new structure. This effect is not observed in our experiments, and we conclude that Lisenkov's model does not apply under the conditions of our study.

We propose an alternative heterogeneous switching model to account for the distinct structural evolution of stripe nanodomains and of the overall superlattice in applied electric fields. Here, the electric field results in the creation and expansion of areas of uniform polarization spatially separated from unswitched regions that remain in the stripe domain phase, as in Fig. 2(d). The characteristic size of switched and unswitched regions during this transition is unknown and requires further investigation. The volume of the switched regions increases, and eventually the sample reaches a homogeneous state of uniform polarization. A complete transition to a uniform polarization state is achieved in electrical measurements with bipolar triangle voltage waveforms in which each voltage polarity is applied for 0.6 ms.

The key prediction of the heterogeneous switching model is that the switched regions are sufficiently large that they are free from the mechanical clamping effect limiting the piezoelectricity of the striped regions and that the switched regions thus exhibit piezoelectric expansion. The difference between the piezoelectric distortion of the domain and superlattice reflections, as in Fig. 2(a), occurs because the domain reflections arise from unswitched regions while superlattice reflections arise from both the switched and unswitched areas. The footprint of the focused x-ray beam is far larger than the 20 nm coherence length of the stripe domain pattern, and x rays diffracted from both unswitched and switched domain regions are detected simultaneously in each diffraction pattern.

The electric-field dependence of the striped-domain dynamics is apparent in measurements of the intensities of the domain reflections during field pulses of several magnitudes. A series of diffraction patterns are shown in Fig. 3(a) at a sequence of times during a 0.84 MV/cm electric field. The intensities of the domain reflections are proportional to the volume of remaining unswitched striped nanodomains, which decreases during the switching process, as shown in Fig. 3(a). Note that the piezoelectricity of the superlattice reflection is not apparent in Fig. 3, an artifact arising

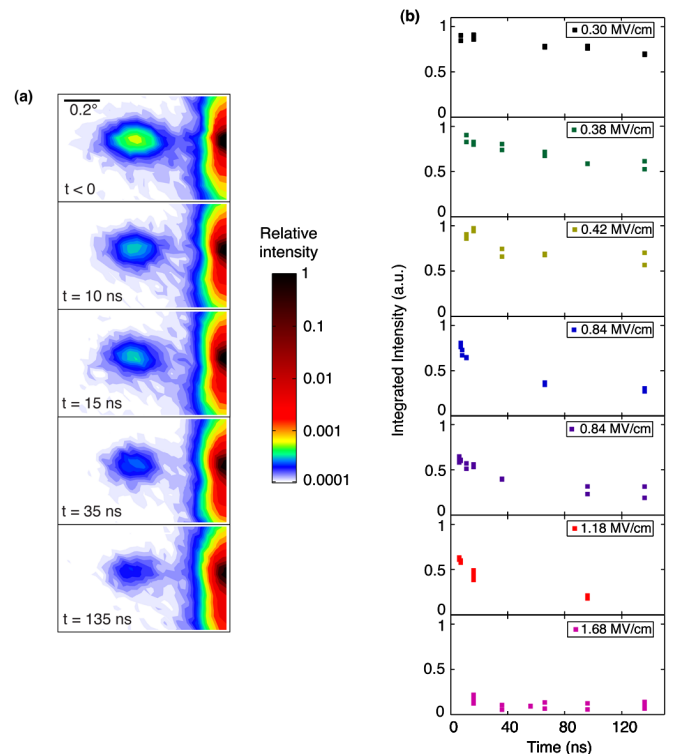


FIG. 3 (color online). (a) Diffraction patterns at several times following the onset of an electric field of 0.84 MV/cm. The patterns show the domain reflection at the center of each image and a tail from a superlattice structural reflection at the right edge of the images. The diffraction patterns were acquired with the diffractometer set for the zero-field Bragg condition. (b) The integrated intensity of the domain satellites as a function of time in electric fields ranging from 0.30 to 1.68 MV/cm.

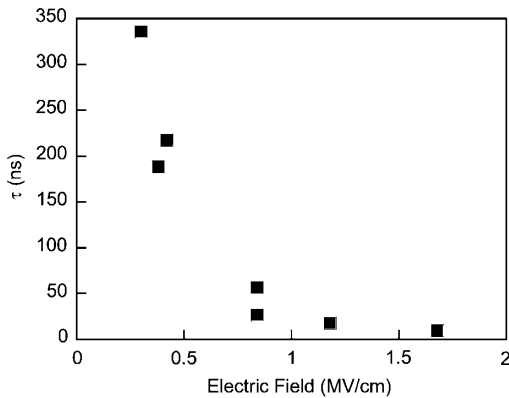


FIG. 4. Characteristic times for the dynamics of the domain reflection as a function of the magnitude of the electric field.

because the  $0.1^\circ$  convergence angle of the incident x-ray beam is sufficient to produce a weak superlattice reflection at these diffractometer settings despite the shift of the peak of the superlattice reflection to lower  $Q_z$ . The monotonic decrease of the integrated intensities of the domain reflections as a function of time is apparent in Fig. 3(b) for several magnitudes of the applied electric field. We have isolated the contribution of the domain reflection to the intensity by subtracting intensities arising from a uniform background and from the tail of the strong superlattice reflection. Domain reflections are evident even after durations as long as 150 ns at electric fields as high as 1.68 MV/cm, indicating that complete conversion to uniform polarization requires longer than this interval.

The magnitude of the electric field has a profound effect on the rate of the change of the intensity of the domain reflection. The time scale for switching was extracted from the data in Fig. 3(b) by fitting the time dependence of the intensity with an exponential decay and extracting time constant  $\tau$ . This exponential, to which we attach no specific physical meaning, is a convenient model-independent approach for extracting the characteristic time for switching. We note that the exponential decay to zero intensity is a poor fit to the data at intermediate electric fields, e.g., 0.84 MV/cm, indicating that the dynamical changes may involve more than one fundamental time scale. The electric-field dependence of the characteristic time  $\tau$  determined in this way is shown in Fig. 4. Increasing the magnitude of electric fields from 0.30 to 1.68 MV/cm reduces  $\tau$  by more than an order of magnitude. For comparison, the coercive field was just 0.25 MV/cm in polarization hysteresis measurements performed at far longer time scales using triangle waveforms with a frequency of 833 Hz, approximately equivalent to pulses of 0.6 ms.

The strong field dependence of the characteristic time for the transformation to the uniform polarization state arises from the competition among the electrostatic energy gained by switching to a uniform polarization state, electromechanical energy, and the electrostatic energy gained by forming nanodomains. The applied field both shifts the minimum-energy state of the system and determines the

kinetics of the switching process, consequently setting its time scale.

In probing the response of the superlattice striped-domain pattern to applied fields, we have found that nanodomains can be manipulated on short time scales, with a proposed mechanism that is quite different than the conventional motion of ferroelectric domain walls. The superlattice dynamics occur with characteristic times that are already as low as several nanoseconds at fields in the MV/cm regime. This effect leads to the possibility that the striped degree of freedom can be manipulated in device structures with gigahertz operating frequencies. Higher fields may open opportunities to understand the coupling between polarization and lattice deformation at time scales down to 1 ns or less.

This work was supported by the U.S. Department of Energy, Office of Basic Energy Sciences, Division of Materials Sciences and Engineering under Grant No. DE-FG02-10ER46147 (P.G.E.). M.D. gratefully acknowledges startup funding from Stony Brook University and technical assistance from Bent Nielsen. Use of the Advanced Photon Source was supported by the U.S. Department of Energy, Office of Science, Office of Basic Energy Sciences, under Contract No. DE-AC02-06CH11357.

---

\*Present address: School of Materials Science and Engineering, Gwangju Institute of Science and Technology, Gwangju 500-712, Korea.

†evans@engr.wisc.edu

- [1] J. B. Neaton and K. M. Rabe, *Appl. Phys. Lett.* **82**, 1586 (2003).
- [2] S. M. Nakhmanson, K. M. Rabe, and D. Vanderbilt, *Appl. Phys. Lett.* **87**, 102906 (2005).
- [3] S. M. Nakhmanson, K. M. Rabe, and D. Vanderbilt, *Phys. Rev. B* **73**, 060101 (2006).
- [4] H. N. Lee *et al.*, *Nature (London)* **433**, 395 (2005).
- [5] M. Dawber *et al.*, *Phys. Rev. Lett.* **95**, 177601 (2005).
- [6] W. Tian *et al.*, *Appl. Phys. Lett.* **89**, 092905 (2006).
- [7] D. A. Tenne *et al.*, *Science* **313**, 1614 (2006).
- [8] S. Lisenkov, I. Ponomareva, and L. Bellaiche, *Phys. Rev. B* **79**, 024101 (2009).
- [9] P. Zubko *et al.*, *Phys. Rev. Lett.* **104**, 187601 (2010).
- [10] V. A. Stephanovich, I. A. Luk'yanchuk, and M. G. Karkut, *Phys. Rev. Lett.* **94**, 047601 (2005).
- [11] S. K. Streiffer *et al.*, *Phys. Rev. Lett.* **89**, 067601 (2002).
- [12] D. D. Fong *et al.*, *Science* **304**, 1650 (2004).
- [13] J. Y. Jo *et al.*, *Phys. Rev. Lett.* **104**, 207601 (2010).
- [14] A. Grigoriev *et al.*, *Phys. Rev. Lett.* **96**, 187601 (2006).
- [15] R. C. Miller and G. Weinreich, *Phys. Rev.* **117**, 1460 (1960).
- [16] L. Chen and A. L. Roytburd, *Appl. Phys. Lett.* **90**, 102903 (2007).
- [17] M. Dawber *et al.*, *Adv. Mater.* **19**, 4153 (2007).
- [18] T. Ejdrup *et al.*, *J. Synchrotron Radiat.* **16**, 387 (2009).
- [19] A. Grigoriev *et al.*, *Rev. Sci. Instrum.* **78**, 023105 (2007).
- [20] A. Grigoriev *et al.*, *Phys. Rev. Lett.* **100**, 027604 (2008).